Remodeling of dermal adipose tissue alleviates cutaneous toxicity induced by anti-EGFR therapy

Leying Chen[1,2], Qing You[1,2], Min Liu[1], Shuaihu Li[1], Zhaoyu Wu[1], Jiajun Hu[1], Liangyong Xia[1], Shiyi Zhang[1*]

[1]School of Biomedical Engineering, Shanghai Jiao Tong University, Shanghai, P. R. China.

[2]These authors contributed equally: Leying Chen, Qing You

Correspondence should be addressed to S.Y.Z. (zhangshiyi@sjtu.edu.cn), School of Biomedical Engineering, Shanghai Jiao Tong University, 800 Dounchuan Road, Shanghai 200240, P. R. China.

Graphical abstract

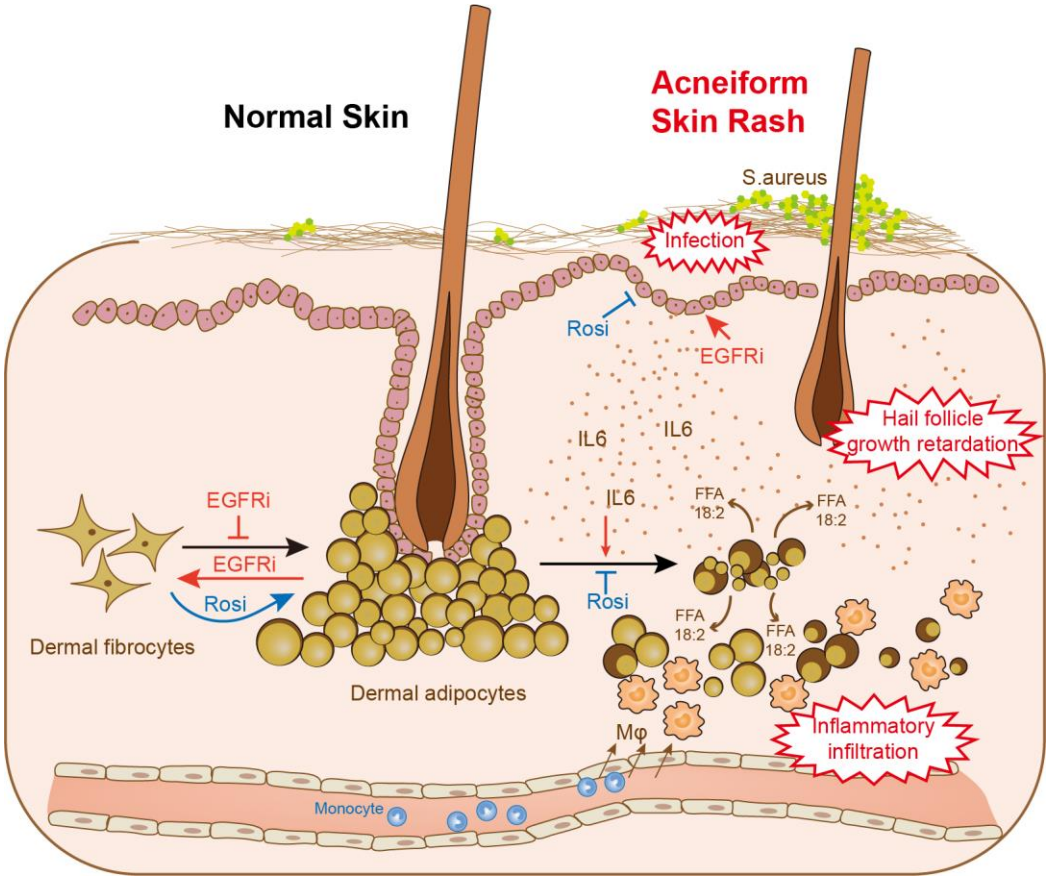

Abstract

Anti-epidermal growth factor receptor (EGFR) therapy–associated cutaneous toxicity is a syndrome characterized by papulopustular rash, local inflammation, folliculitis and microbial infection, resulting in a decrease in quality of life and dose interruption. However, no effective clinical intervention is available for this adverse effect. Here, we report the atrophy of dermal white adipose tissue (dWAT), a highly plastic adipose tissue with various skin-specific functions, correlates with rash occurrence and exacerbation in a murine model of EGFR inhibitor-induced rash. The reduction in dWAT is due to the inhibition of adipogenic differentiation by defects in peroxisome proliferator-activated receptor γ (PPARγ) signaling, and increased lipolysis by the induced expression of the lipolytic cytokine IL6. The activation of PPARγ by rosiglitazone maintains adipogenic differentiation and represses the transcription of IL6, eventually improving skin functions and ameliorating the severity of rash without altering the antitumor effects. Thus, activation of PPARγ represents a promising approach to ameliorate cutaneous toxicity in patients with cancer who receive anti-EGFR therapy.

Introduction

Epidermal growth factor receptor (EGFR) is a canonical therapeutic target for non-small cell lung cancer, breast cancer and colorectal cancer. Cutaneous toxicity induced by EGFR inhibitors (EGFRIs) is an inflammatory disorder characterized by papulopustular rash, folliculitis, microbial infection and pruritus. Most commonly, rash is observed in 70-90% of patients receiving anti-EGFR therapy(Cappuzzo et al., 2010; Mok et al., 2017; Sequist et al., 2013), resulting in a decrease in quality of life. Except for the empiric use of corticosteroids and antibiotics, no effective clinical treatment is currently available for these adverse effects, which is responsible for 8-17% of dose modifications and interruptions(Lacouture, 2006). Therefore, new therapeutic targets for EGFRI-specific skin toxicity urgently need to be discovered.

Dysfunction of the epidermal barrier, retardation of hair follicle growth and various dermal inflammatory responses have been proposed as causative factors for EGFRI-induced rash, but therapeutic agents that interfere with these mechanisms have limited effectiveness(Lichtenberger et al., 2013; Mascia et al., 2013). An analysis of biopsies from rodents with the genetic ablation of EGFR or pharmacological EGFR inhibitors both showed a dramatic loss of dermal adipose tissue(Murillas et al., 1995; Sibilia and Wagner, 1995; Sugawara et al., 2010; Surguladze et al., 2009), a newly recognized adipose layer termed dermal white adipose tissue (dWAT). Compared to other conventional fat depots, dWAT has more skin-specific functions and a high plasticity to expand or contract in response to different stimuli(Chen et al., 2019). For example, local infection(Zhang et al., 2015), a high-fat diet (HFD) and peroxisome proliferator-activated receptor γ (PPARγ) agonists(Z. Zhang et al., 2019) induce dWAT expansion. Recent studies have revealed unique roles for dWAT in skin fibrosis and scarring(Marangoni et al., 2015; Varga and Marangoni, 2017; L. juan Zhang et al., 2019), wound healing(Plikus et al., 2017; Schmidt and Horsley, 2013; Shook et al., 2020), immune modulation(Dokoshi et al., 2018; Schmid

et al., 2017; Zhang et al., 2015), and regeneration of hair follicles(Donati et al., 2014; Festa et al., 2011). During the hair cycle, dermal adipose tissue expands in the anagen phase and regresses in catagen phase, providing vital signals to regulate hair growth(Z. Zhang et al., 2019). In addition, the reduction in dWAT in transgenic and pharmacologically treated mice results in a scaly skin phenotype with delayed hair coat formation, poorly developed pilosebaceous structures and epidermal barrier function(Chen et al., 2002; Herrmann et al., 2003), and these phenomena resembled the abnormalities in skin observed upon EGFR inhibition. A similar synchronized pattern was also observed in wound healing. Dermal adipocytes surrounding the site of skin injury undergo lipolysis and dedifferentiation, transition to myofibroblasts and attract macrophages to stimulate re-epithelialization and revascularization(Shook et al., 2020). Additionally, new adipocytes regenerating from myofibroblasts were also observed in healed wounds(Plikus et al., 2017). The importance of dWAT in host defense is the promotion of cathelicidin antimicrobial peptide (Camp) release during adipogenic differentiation(Zhang et al., 2015). The production of Camp defends against *Staphylococcus aureus* (*S. aureus*) infection, which often develops along with EGFRI skin toxicities(Lichtenberger et al., 2013).

Since the multiple functions of dWAT are closely related to EGFRI-induced skin toxicities and a reduction in dermal fat has been observed in EGFR-depleted mice, we investigated whether dWAT plays a central role in EGFRI-induced rash. Here, using an EGFRI-induced rash model and dermal fibroblast (dFB) differentiation assays, we showed that atrophy of dWAT occurs during rash development and has a strong causality with rash severity. The differentiation of dFBs was obviously inhibited and lipolysis of mature adipocytes was increased upon EGFR inhibition. Notably, stimulating dermal adipocyte expansion with a high-fat diet (HFD) or the pharmacological PPARγ agonist rosiglitazone (Rosi) ameliorated the severity of rash.

Materials and Methods

Animal models and treatment

Female 6-8 weeks SD rats and neonatal rats were obtained from Jihui, Shanghai, China. Female 3-week SD rats were purchased from Charles River, Beijing, China. 6-week BALB/c nude mice were from Jihui, Shanghai, China. Rash model was generated by daily p.o. of Afatinib at a dose of 40 mg/kg for about 10 consecutive days, the back hair was gently shaved for observation.

For HFD experiment, 3-week rats were fed with a HFD diet for 5 weeks to induce the expansion of the dWAT layer, then followed with Afatinib treatment to construct rash model. For rosiglitazone application experiment, vehicle gel or rosiglitazone gel (made of propylene glycol, transcutol, PEG400, water, carbopol 980 and 1% rosiglitazone) was applied topically on the shaved back of rat, the rats were fixed in a cylindrical holder for four hours during the application, and then the residual ointment was removed. The back skin changes were visually inspected every day.

For dWAT ablation experiment, deoxycholic acid (vehicle: 0.9% benzyl alcohol in PBS) was

intradermal injected in rat back skin every three days, each rat received 2.5 mg/cm^2 deoxycholic acid for 9 times.

To develop xenograft tumor transplanting mice model, a single-cell suspension of 5×10^6 PC9 cells was inoculated subcutaneously into each nude mouse. After 3 weeks, oral gavage of 30mg/kg afatinib and topical application of vehicle or rosiglitazone gel were started when tumor volume reached 100 mm^3.

Reagents

Afatinib and rosiglitazone were purchased from Goyic, China. Propylene glycol was from ER-KANG, China. Transcutol was from GATTEFOSSé, French. Carbopol 980 was from 2Y-Chem, China. PEG400 was from YIPUSHENG, China. Dexamethasone (D4902), indomethacin (I8280), recombinant human insulin (407709) and 3-isobutyl-1-methylxanthine (IBMX) (I7018), Isoproterenol (1351005) were from Sigma. The anti-PDGFR alpha (ab203491) and anti-ATGL (ab109251) antibodies were from Abcam. The anti-caveolin-1 (3267), anti-phospho-AKT1 (5012), anti-AKT1 (2938), anti-phospho-AKT2 (8599), anti-AKT2 (3063) antibodies were from Cell Signaling Technology. The anti-phospho-HSL (abs139855) was from Absin. The anti-HSL antibody (NB110-37253) was from Novus. The anti-PDGFR alpha antibody (ab203491) was from Abcam. The GAPDH antibody (60004-1-lg) was from Proteintech. The secondary antibodies used were from Beyotime. BODIPY 493/503 (D3922) was purchased from ThermoFisher. Deoxycholic acid (D2510) was obtained from Sigma. Human IL6 (200-06) was from PeproTech.

Cell culture

HaCaT and PC9 cells were cultured in DMEM/high glucose medium, THP-1 cells were cultured in 1640 complete medium, all supplemented with 10% fetal bovine serum (FBS) and 1% penicillin-streptomycin in an incubator under a humidified atmosphere of 5% CO2 at 37°C.

Rash grade evaluation

Grade 0-normal; Grade 1-papules and/or pustules covering $<$ 10% surface area of shaved-back skin; Grade 2-papules and/or pustules covering 10-30% surface area of shaved-back skin; Grade 3-papules and/or pustules covering $>$ 30% surface area of shaved-back skin.

Histology, immunohistochemistry (IHC) and immunofluorescence (IF)

Rat skin was embedded by paraffin or OCT and sectioned for staining. H&E staining was performed using paraffin sections. Oil red and Ki67 were directly stained using OCT sections. For IHC and IF, paraffin or OCT sections were fixed and blocked, then stained with CD68 or caveolin-1 primary antibody followed by secondary antibodies. Nuclei were counter-stained with DAPI. All images were scanned with a digital pathology scanning system (NANOZOOMER S360, Leica) or Upright-Reverse Fluorecent Microscopy (Revolve, Echo).

Dermal adipocytes and primary dermal fibroblasts isolation and culture

Neonatal (P1) and adult rat back skin was cut into small pieces then digested with Liberase TL (Roche) for 1 hour at 37°C with constant shaking. Cells mixture was first filtered through 70 μm filter to discard tissue pieces, floating dWAT was collected by centrifuging and followed by washing. Cell suspension was then treated with red blood cell lysis and washed with PBS. dFB suspension was obtained by filtering through 40 μm filter. Isolated dFB was cultured in DMEM supplemented with 10% FBS in a humidified incubator at 5% CO_2 and 37°C. Fresh medium was changed daily and only one passage was used for experiment. To induce adipocyte differentiation, post-confluent dFB was switched to adipocyte differentiation medium containing 2 μM Dexamethasone, 250 μM IBMX, 200 μM Indomethacin and 10 μg/mL recombinant human insulin for 9 days. 10 nM Afa or 5 μM Rosi was added in differentiation medium and changed with fresh differentiation medium at day 3, 6 and 9.

dWAT dedifferentiation was demonstrated using ceiling culture. Briefly, isolated dWAT was transferred to an inverted 25-cm^2 cell culture flask, completely filled with DMEM supplemented with 20% fetal bovine serum and Afa or Rosi. Adipocytes were monitored daily for cell attachment. After sufficient attachment and occurrence of dedifferentiated adipocytes, medium was removed, replaced with fresh medium and the flask was reinverted.

For confocal microscopy, dFB cells were cultured, differentiated, and treated with HaCaT supernatants in 12-well cell culture slides. Lipids were stainted with BODIPY 493/503. Cell nucleus were stained with stained with DAPI Fluoromount-G (Yeasen). Microscopy was performed on Leica TCS SP8.

Cell proliferation assay

Cells were cultured in 96-well plate and treated with different agents. Twenty-four hours after treatments, cells were counted using Cell Counting Kit-8 (Yeasen).

Flow cytometry and analysis (FACS)

Freshly isolated dFB from rat skin was stained with zombie violet viability dye (Biolegend, 423114) to stain dead cells. Cells were then stained with an antibody cocktails containing PE-CD31 (BD, 555027), FITC-CD45 (BioLegend, 202205), PerCP/Cy5.5-CD29 (BioLegend, 102227), and PE-Cy7-CD34 (SantaCruze, sc-7324). FACS analysis for protein expression of each cell marker was performed by the BD FACSCanto RUO machine and analyzed by FlowJo V10 software.

Transmission electron microscopy (TEM)

TEM was performed in the Instrumental Analysis Center of SJTU. Vehicle and Afa rats were anesthetized after 5-days oral gavaged and immediately transcardially perfused using PBS, then 50ml of cold 4% PFA. The vehicle control and Afa-induced rash back skin were dissected and cut into small pieces, approximately 1mm^3 in volume. Tissue pieces were fixed in 2.5% glutaraldehyde for 30 min at RT and 1.5 hours at 4°C, and then rinsed

in PBS three times. Samples were postfixed in 1% osmium tetroxide for 1 hour, rinsed and enbloc stained in aqueous 2% uranyl acetate for 1 hour followed by rinsing, dehydrating in an ethanol and acetone series, infiltrating with resin and baking 48 hours at 60°C. Hardened blocks were cut using an ultramicrotome (Leica EM UC7). Ultrathin 100 nm sections were collected and stained using lead citrate for transmission microscopy. Carbon-coated grids were viewed on a transmission electron microscope (Talos L120C G2) at 120kV.

Lipolysis assay

For *ex vivo* lipolysis assay, sWAT explants were collected and cultured in 12-well plate, for *in vitro* lipolysis assay, differentiated adipocytes were cultured in 24- well plate, cells and explants were cultured in serum-free DMEM containing 2% fatty acid- free BSA. 10 μM Isoproterenol was added to induce lipolysis, cells and explants were treated with Afa. Glycerol was measured after different hours stimulation at 37°C with shaking. The glycerol assay (Sigma) or NEFA assay (Wako Diagnostics) was used to measure lipolysis, as per manufacturer's instructions.

Lipid profiling

For quantitative lipid mass spectrometry of adipocyte lipid stores, dWAT of vehicle control and Afa was digested with Liberase TL as described above. Isolated dWAT was washed with HBSS and 10^6 cells were counted for each sample, total lipids were extracted and FA profiles were quantified by GC/MS.

***S. aureus* assay**

Skin biopsies were homogenized in PBS by Precellys Evolution homogenizer (Bertin; 2× 30 s at 6000 rpm followed by 30 s on ice after each cycle). 100 μL homogenized skin samples were plated onto *S. aureus* color culture medium (Comagal, France) and counted after 24 hours culture at 37°C.

Migration assay

THP-1 migration assay was performed using transwell chamber with 8 μm pore size (Falcon) for 24-well plates. 500 μL of dFB-derived supernatant was loaded in the lower chamber. 200 μL Calcein-AM (Yeasen) –labelled cell suspension was added to the upper chamber. The chamber was incubated at 37°C for 3h in a CO_2 incubator. After incubation, THP-1 cells that migrated to the lower chamber were counted under a microscope.

Western blot

Cells were lysed using RIPA lysis buffer. Proteins were separated on 7.5-10% SDS-PAGE gel and transferred to PVDF membrane. The membranes were blocked for 1 hr in TBST containing 5% BSA, and then incubated with primary antibodies overnight. The membranes were then washed with TBST for 10 min x 3 times, and incubated in secondary antibodies for 1 hr. Membranes was washed again with TBST for 20 min x 3 times and revealed using the Super Signal West Pico kit (Thermo Scientific).

Quantitative PCR

RNA was extracted from rat skin and indicated cells using the TRIzol Reagent (Invitrogen). cDNA was generated from total RNA using a ReverTra Ace qPCR RT Master Mix (FSQ-201, TOYOBO) according to the manufacturer's instructions. Quantitative real-time PCR was performed with the ABI ViiA7 or ABI 7500 Realtime PCR system using SYBR Green Master Mix (YEASEN). The primers used for amplification of specific genes were synthesized by Sangon (Supplementary file 4).

Enzyme-linked immunosorbent assay

Quantification of Human IL6 protein concentrations in HaCaT culture supernatants, and Rat IL6 from rat skin homogenates were performed by enzyme-linked immunosorbent assay (ELISA) according to the Human/Rat IL6 ELISA kit protocol (Boster).

Blood biochemistry test

Blood samples were collected into the EDTA-K2 anticoagulative tubes to measure blood routine examination by SYSMEX POCH100IVD. For lipid level examination, blood samples were centrifuged at 3000 g for 10 min to separate serum, the serum lipid were detected by Adicon, Ltd.

Statistical

Statistical analysis was performed using unpaired Student's *t* test or one-way analysis ANOVA. Differences were considered significant when *P* was less than 0.05: $*P < 0.05$; $**P < 0.01$; $***P < 0.001$.

Data availability statement

All data supporting the findings of this study are provided within the paper and its supplementary information. All additional information will be made available upon reasonable request to the authors. Source data are provided with this paper.

Results

A reduction in dWAT is a hallmark of the pathophysiology of rash. EGFRI therapy in patients is consistently associated with specific skin toxicities, such as papulopustular rash. Additionally, weight loss and decreased appetite accompany these changes (Supplementary file 1). Recent reports have shown a strong, positive correlation between body weight and dWAT thickness(Kasza et al., 2016). To investigate whether dWAT responses to EGFR inhibition, we established a rat rash model by repeated oral gavage of afatinib (Afa), an EGFR inhibitor with a high occurrence of skin toxicity(Sequist et al., 2013). Rats continued losing weight and exhibited reduced food intake throughout the Afa intervention, and at the end of the treatment, they had lost up to 27.9% and 23.1% of their initial body weight and food intake, respectively (Figure S1A and 1B). The rat model recapitulated all skin features of patients receiving EGFRIs, including erythema, pustules and itching, and the pustules conflated to lakes of pus that dried and formed yellow crusts when rash developed to a higher grade (Figure 1A). During rash occurrence, the thickness

of the dWAT layer decreased with an increase in the rash grade, and skin lipid levels also decreased (Figure 1B and 1C). A significant decrease in the number of cells stained with the adipocyte surface protein Caveolin-1 was also observed (Figure 1D).

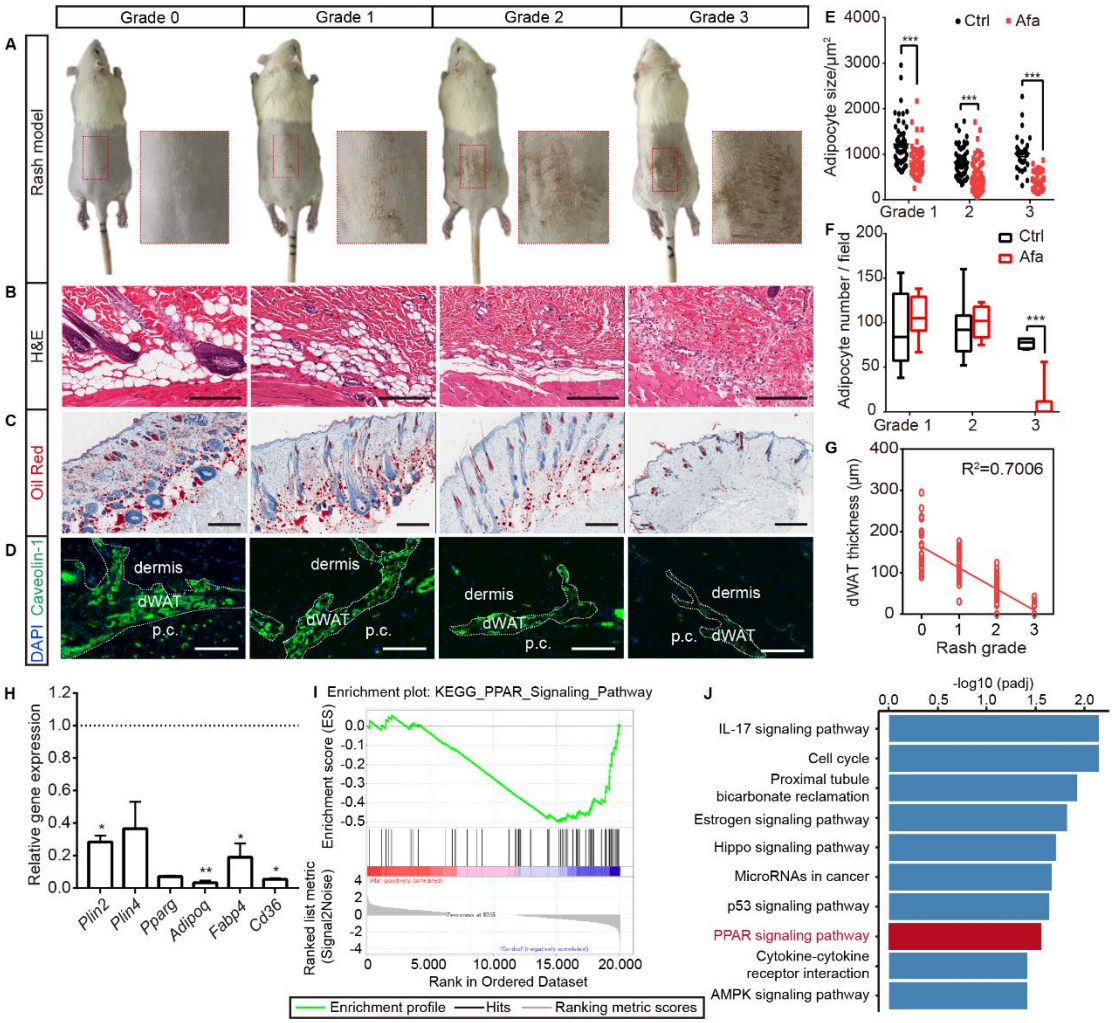

Figure 1 The response of dWAT to EGFR inhibition.

(A) Representative images of the rat rash model. (B-D) H&E (B), Oil Red (C), and Caveolin-1 (D) staining of skin from control and Afa-treated rats. Scale bars: 200 μm, 500 μm and 130 μm (top to bottom). p.c. refers to panniculus carnosus. (E and F) Quantification of the dWAT size (E), and adipocyte number (F) in rats with different rash grades compared with the control (Ctrl). *n*=3-5 per group. (G) Relationship between dWAT thickness and rash grade. The square values of the Pearson's correlation coefficients are shown. (H) RT-PCR measurements of mRNA levels of adipogenic genes in skin tissues from control and Afa-treated rats. *n*=4-5 per group. (I) Gene set enrichment analysis (GSEA) of the gene signatures of PPAR signaling in Afa-treated skin compared with the Ctrl. NES, normalized enrichment score. (J) The top 10 enriched KEGG pathways. Data are presented as the means ±SEM. *P < 0.05, **P < 0.01, and ***P < 0.001 using 2-tailed unpaired Student's t test.

Changes in dWAT were examined by performing a detailed morphometric analysis. The attenuation of intradermal adipocytes was due to a decrease in both size and number, and time-course studies revealed that the size change occurred prior to the change in adipocyte number (Figure 1E and 1F). Consistent with our hypothesis, a positive

correlation existed between dWAT thickness and rash grade throughout Afa treatment (Figure 1G). This correlation suggests that changes in the dWAT layer in response to a process associated with EGFRI affected skin function. In addition to the dermal adipose layer, skin-associated adipose tissue also includes back subcutaneous adipocytes (sWAT), inguinal adipocytes (iWAT) and brown adipocytes (BAT), which are all adjacent to the back skin. Although clear evidence of anatomically and functionally distinct skin adipose depots in rodents has been reported, for example, the dWAT layer was separated by a distinct muscle layer known as the panniculus carnosus and verified to develop independently of sWAT, these two layers are not quite physically and functionally demarcated in humans(Chen et al., 2019; Wojciechowicz et al., 2013). Thus, we also monitored the weight change of sWAT and other skin adipose depots, and found that iWAT and BAT also showed a decreasing trend at late time points (Figure S1C), whereas sWAT represented a more similar response to dWAT during rash occurrence (Figure S1D-S1F).

The reduction in the size and number of adipocytes in the dWAT layer at the rash site suggested that adipocytes may be modulated by the inhibition of differentiation and an increase in lipolysis. To examine whether the differentiation of dermal adipocyte was affected, we first compared the expression of differentiation-associated genes in Afa-treated skin with that in vehicle-treated skin using quantitative PCR. The expression of general adipocyte marker genes were significantly decreased at the end of the treatment (Figure 1H). Additionally, our previous study revealed an enrichment of genes in PPAR signaling after Afa treatment based on GSEA and KEGG pathway annotations (Figure 1I and 1J). Taken together, these data suggest that the loss of dermal adipocytes is a characteristic hallmark of EGFRI-induced skin toxicity, and this process might be modulated by PPAR-mediated differentiation.

EGFRI stimulation induces the dedifferentiation of dWAT. A loss of dWAT was also reported to be a prominent feature of systemic sclerosis in humans, a disease with disturbed skin homeostasis and dermal fibrosis. The adipocyte–myofibroblast transition is the primary event in the pathogenesis of cutaneous fibrosis(Varga and Marangoni, 2017). Additionally, dermal adipocyte dedifferentiation and subsequent conversion to myofibroblasts have been verified in skin injury and are necessary for efficient tissue repair(Shook et al., 2020). To characterize dermal adipocyte differentiation, we first performed Masson's trichrome staining for collagen to characterize dermal adipocyte differentiation. Rats receiving daily Afa treatments showed a time-dependent progressive decrease in dWAT thickness associated with a slightly thicker dermis and collagen deposition in the early stage of rash (Figure 2A and 2B). We next analyzed the expression of fibrotic genes in dWAT before and after rash to evaluate the adipocyte to fibroblast transdifferentiation process. However, dermal adipocytes isolated from the back skin of Afa-treated rats only exhibited slight fibrotic potential in the early stage that diminished quickly (Figure 2C), whereas the expression of general adipocyte markers represented a continuous and obvious decrease (Figure 2D). The same trend was also observed in sWAT (Figure S2A and S2B). These data suggest that collagen deposition and myofibroblast transition occur in the early phases of EGFRI-related skin changes and are sustained for only a short period.

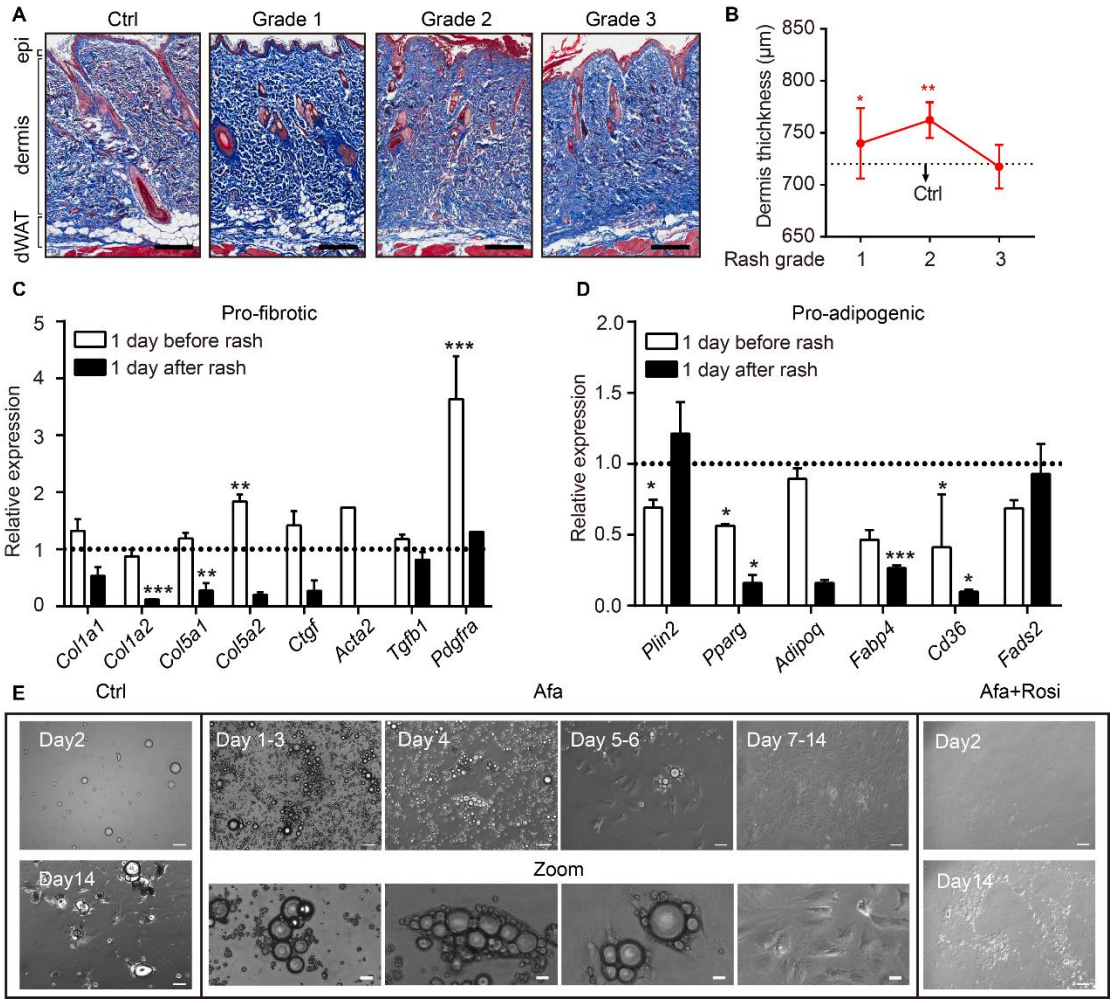

Figure 2 Dedifferentiation of mature dermal adipocytes upon EGFR inhibition

(A) Masson's trichrome staining of skin sections from rats at the indicated times. *n*=3-5 per group. epi refers to epidermis. Scale bars: 500 μm. (B) Changes in the thickness of the dermis in Ctrl- and Afa-treated rats. *n*=3-5 per group. (C and D) RT-PCR measurements of profibrotic genes (C), and proadipogenic genes (D) in isolated dermal adipocytes at the indicated times, *n*=3-4 per group. (E) Morphological changes at different time points of Afa (100 nM) or Rosi (5 μM) treatment revealed a transition from mature dermal adipocytes to dedifferentiated adipocytes. Scale bars: 100 μm and 50 μm for zoom pictures. Data are presented as the means ±SEM. *P < 0.05, **P < 0.01, ***P < 0.001 using 2-tailed unpaired Student's t test.

To determine whether dedifferentiation exists, ceiling culture was performed using dWAT cells isolated from normal rat back skin. Upon EGFRI stimulation, we found that attached adipocytes began to decrease the size of lipid droplets and the cells formed spindle-like shapes on day 4 after Afa treatment. Then, they gradually elongated, lost intracellular lipids and proliferated as fully dedifferentiated PDGFRα+ fibrocytes (Figure 2E; Figure S2C). In comparison, adipocytes cultured under control experimental conditions attached two days later and retained lipid droplets for several days (Figure 2E). Based on our evidence, the expression of genes related to the function of mature adipocytes, such as *PPARg*, *Adipoq*, and *Fabp4,* was downregulated after EGFRI treatment (Figure 1H; Figure 2D). The gene enrichment analysis highlighted the significance of PPAR signaling

in the pathology of EGFRI-induced skin toxicity. The blockade of PPARγ produces defective adipocytes and exerts a negative effect on skin wound healing(Schmidt and Horsley, 2013). In contrast, rosiglitazone (Rosi), a PPARγ agonist, abrogates bleomycin-induced scleroderma and blocks profibrotic responses(Bi et al., 2016; Wu et al., 2009). Thus, we hypothesized that PPARγ upregulation might reverse adipocyte dedifferentiation in response to EGFR inhibition through a compensatory mechanism. We evaluated the effect of Rosi on Afa-treated dermal adipocytes to directly test this hypothesis. Application of Rosi reversed the dedifferentiation of dermal adipocytes induced by Afa, and cells cultured in the presence of Rosi displayed little attachment until 14 days (Figure 2E). In summary, these results suggest that an EGFR signaling deficiency, caused by treatment with EGFRI, triggers dermal the adipocyte-myofibroblast transition at an early stage and significant dedifferentiation, and the PPARγ agonist Rosi effectively rescues this phenomenon.

Differentiation of adipocyte precursors are suppressed during EGFR inhibition. Dermal adipocyte precursor cells (APs) were recently identified in the skin(Festa et al., 2011); moreover, recent genetic and molecular research revealed that the activation of APs depends on the PDGFRA-PI3K-AKT pathway(Rivera-Gonzalez et al., 2016). The AKT pathway is a key downstream target of EGFR kinase, which also modulates proliferation and survival. To determine whether the loss of mature dWAT cells was caused by EGFR inhibition on APs, we isolated dFBs from the skin dermis and treated them with Afa for 3, 6 and 9 days during adipogenic differentiation *in vitro*. Consistent with our hypothesis, the differentiation of dFBs in the presence of Afa was inhibited (Figure 3A), and the concentration of Afa used in this experiment had little antiproliferative effect (Figure S3A). Notably, the addition of Rosi circumvented the inhibition of adipogenic differentiation (Figure 3A). Next, we aimed to define the molecular pathways affected by EGFR inhibition in dermal adipogenic cells. The gene signature induced by Afa in APs (Figure 3B) was similar to the changes in gene expression observed in mature adipocytes (Figure 2D). Adipocytes have been shown to express a variety of pattern recognition receptors and cytokine receptors, including TLR1-9, NOD1-2, TNFR, IL4R and IL6R(Chen et al., 2019; Deiuliis et al., 2011; Sindhu et al., 2015). Interestingly, the expression levels of many of these receptors were increased during Afa treatment (Figure S3B), indicating the proinflammatory potential of adipocytes upon EGFR inhibition. Additionally, we analyzed the levels of PDGFRα and phosphorylated AKT. Significantly increased levels of PDGFRα were detected on days 6 and 9, indicating a retardation of AP differentiation. Phospho-AKT1 and phospho-AKT2 levels were also affected by Afa (Figure 3C). Cotreatment with the PPARγ agonist Rosi and the EGFR inhibitor Afa completely abrogated the inhibition of APs differentiation. Notably, the addition of Rosi significantly activated both AKT1 and AKT2 (Figure 3C). We next examined the number of APs in EGFRI-treated rats. Using FACS, we found that APs ($CD31^-$, $CD45^-$, $CD34^+$, $CD29^+$) were absent after EGFR inhibition (Figure 3D and 3E). Together, these data indicate that the loss of mature dermal adipocytes induced by an EGFRI correlates with loss of APs and inhibition of their activation.

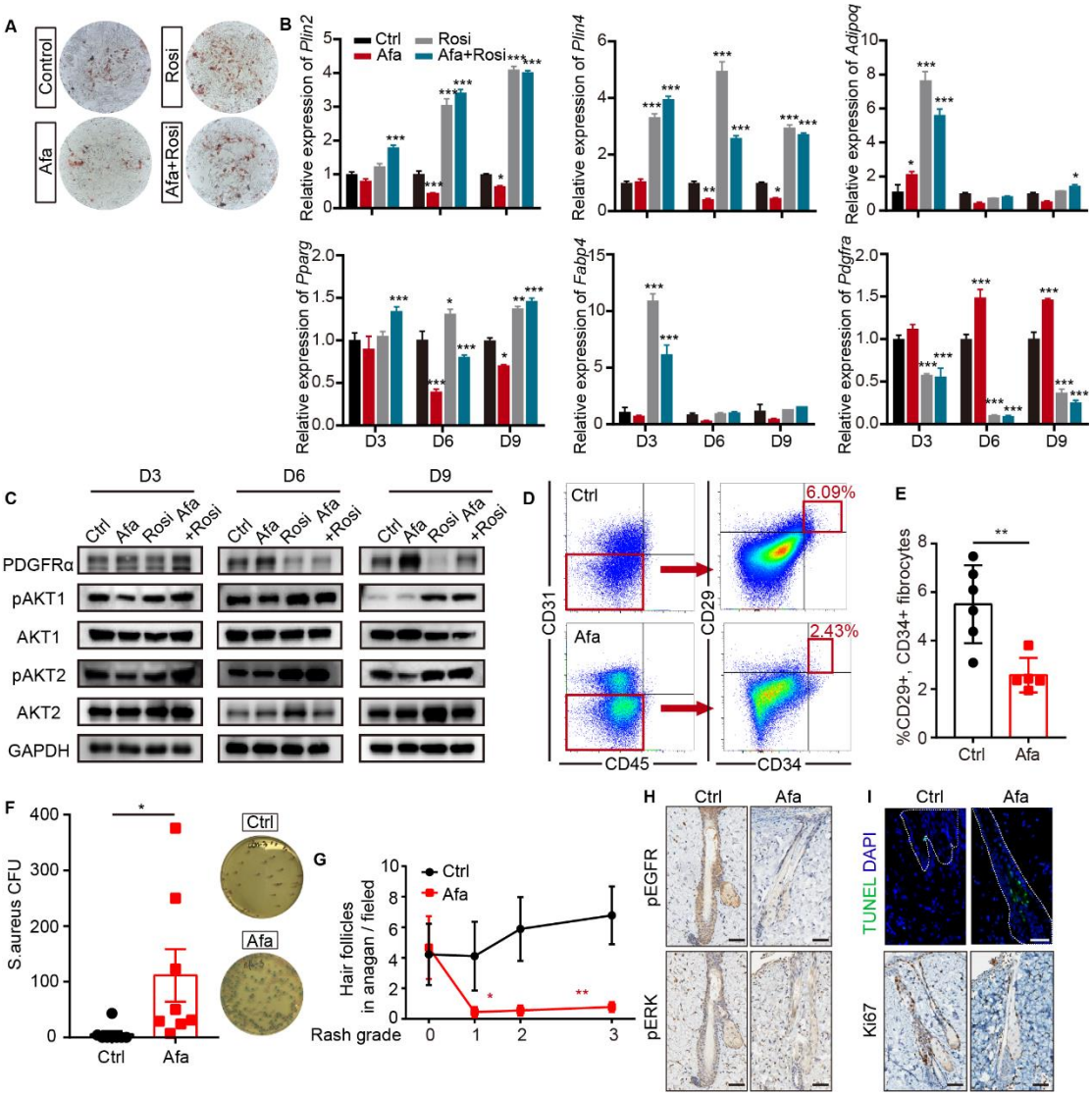

Figure 3 EGFR inhibition blocks adipocyte progenitor differentiation

(A) dFB cells were isolated from P1 rat skin and then cultured with adipocyte differentiation medium for 9 days in the presence or absence of Afa (10 nM) or Rosi (5 μM). Lipid production was detected using Oil Red staining. (B) Relative mRNA expression of adipogenic genes at the indicated time points during differentiation. *n*=3 per group. (C) Western blot analysis of differentiating dFB cells. (D) FACS analysis of adipocyte progenitors in dFB from Ctrl- and Afa-treated rats. (E) The percentage of $CD31^-$, $CD45^-$, $CD34^+$ and $CD29^+$ fibrocytes was quantified. *n*=5-6 per group. (F) *S. aureus* growth in media containing skin homogenates from Ctrl- or Afa-treated rats. *n*=8 per group. (G) Numbers of hair follicles in anagen phase during Afa treatment. *n*=3 per group. (H and I) Immunostaining for pEGFR and pERK (H), Ki67 and TUNEL (I) in skin biopsies from Ctrl- and Afa-treated rats. *n*=3 per group. Scale bars: 50 μm. Data are presented as the means ±SEM. *P < 0.05, **P < 0.01, and ***P < 0.001 (Afa/Rosi group *vs* Ctrl group and Afa+Rosi group *vs* Afa group) using 2-tailed unpaired Student's t test and one-way ANOVA.

Since recent reports have shown that dermal adipocytes have the capacity to inhibit invasive bacterial skin infection and support hair regeneration(Festa et al., 2011; Zhang et al., 2015), we determined whether the reduction and inhibition of APs contribute to the loss of these functions. As expected, impaired dermal adipogenesis resulted in increased *S.*

aureus infection (Figure 3F). In addition, the number of hair follicles in anagen phase decreased with an increasing rash grade (Figure 3G), and rats treated with the EGFRI showed hair follicles with abnormal growth (Figure 1B). The levels of phospho-EGFR and ERK in the outer sheath of hair follicles were significantly decreased (Figure 3H). Consequently, the number of proliferative cells characterized by Ki67 immunostaining was reduced, and the number of apoptotic cells detected using TUNEL immunofluorescence staining was increased (Figure 3I). Therefore, a lack of APs and mature dWAT impairs the maintenance of the host defense and hair growth in the skin.

EGFR inhibition induces lipolysis through epidermal keratinocytes. In addition to differentiation, the reduction in dermal adipocyte size also suggested that adipocytes might alter their lipid content through lipolysis. To examine whether lipolysis occurs after EGFR inhibition, isolated dermal adipocytes were assessed using transmission electron microscopy, and the expression of lipolysis-activated markers, the rate-limiting enzyme ATGL and phosphorylated hormone-sensitive lipase (pHSL) were detected. We observed increased levels of ATGL and pHSL in dWAT (Figure 4A and 4B). Consistent with these changes, multiple smaller droplets adjacent to large lipid droplets were detected in Afa-treated rats, whereas only large, unilocular lipids were retained in the control group (Figure 4C). However, in sWAT, lipolysis-induced glycerol production was not increase in either sWAT isolated from Afa-treated rats or Afa stimulation of sWAT from Ctrl-treated rats (Figure S4A). We performed lipidomics on isolated dermal adipocytes from Ctrl- or Afa-treated rats to characterize the composition of fatty acids (FAs). The fatty acid composition of adipocytes from Afa- or Ctrl-treated rats did not show any significant differences, and the only significantly changed medium-chain FA was decanoic acid (10:0) (Figure S4B and S4C). Notably, the most abundant FAs were mainly C18 fatty acids, including methyl oleate (18:1), methyl elaidate (18:1T), methyl linoleate (18:2) and methyl linoelaidate (18:2T) (Figure S4C), indicating the extensive release of these types of FAs to the cell matrix during lipolysis. Correspondingly, the free fatty acid (FFA) in the skin homogenates showed an enrichment in Afa-treated rats (Figure S4D). Experimental studies support the hypothesis that lipolysis-induced lipid accumulation drives macrophage infiltration(Kosteli et al., 2010; Shi et al., 2006). Lipolysis and a decrease in adipocyte size corresponded with the infiltration of macrophages when rash occurred (Figure 4D and 4E). We hypothesized that individual FA components might promote the migration of macrophages. Monocytes have been well known migrated to local inflammatory sites and differentiated to macrophages. Thus we treated human monocyte THP-1 cells with one significantly changed FA, decanoic acid (10:0), or the other four most abundant C18 FAs to verify this hypothesis. In particular, we observed that the number of migrated monocytes was increased in the 18:2-treated wells (Figure S4E and S4F).

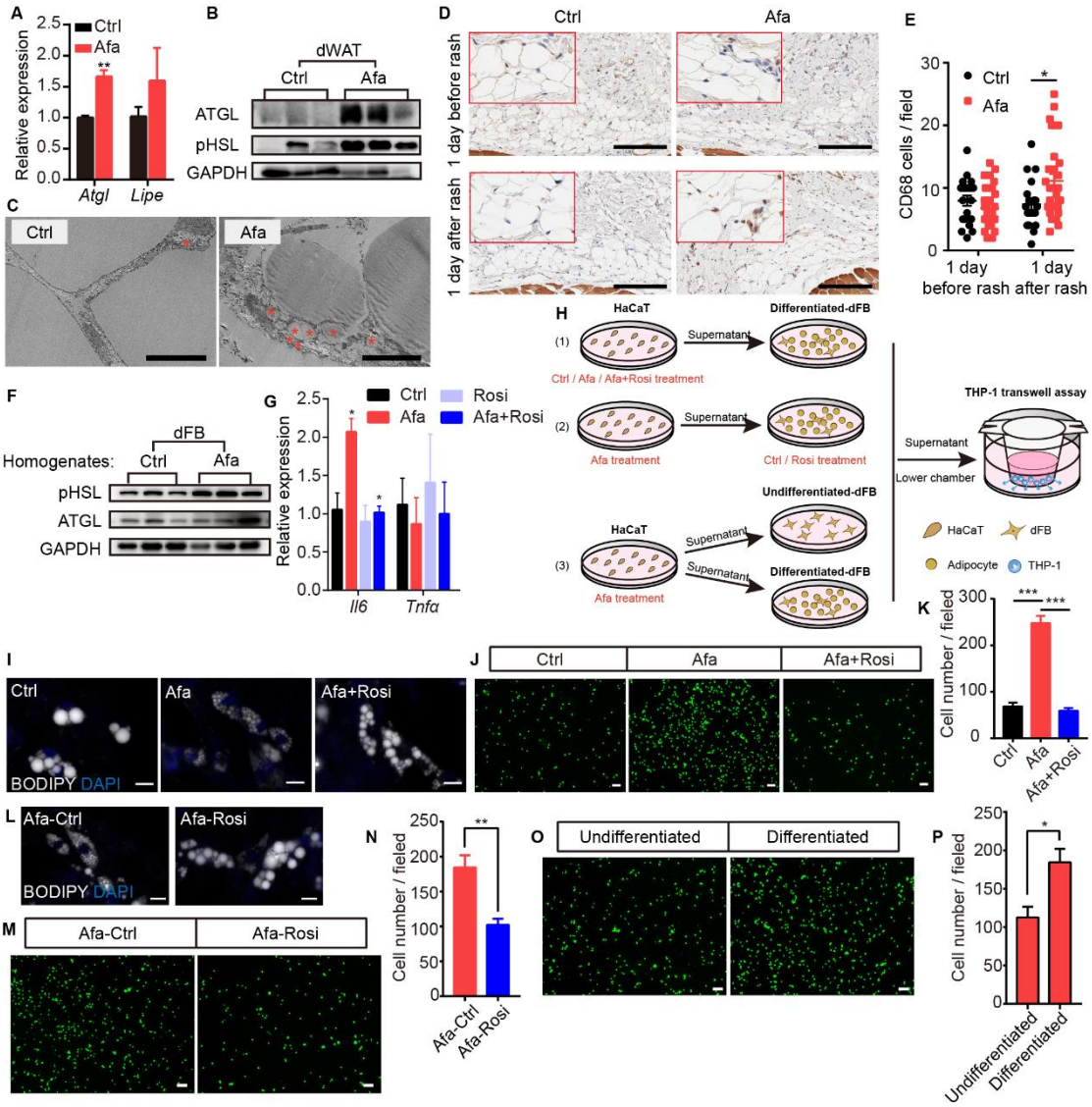

Figure 4 EGFR inhibition blocks adipocyte progenitor differentiation

(A) Relative expression of the *Atgl* and *Lipe (Hsl)* mRNAs in isolated dWAT on day 5. *n*=3 per group. (B) Western blot of lipase level from isolated dWAT cells at Grade 1. (C) Transmission electron microscopy images of dermal adipocytes from Ctrl- and Afa-treated rat skin on day 5. Asterisks show small lipid droplets. Scale bars: 5 μm. (D and E) Representative images of CD68 immunostaining (D) and quantification (E) in skin from Ctrl- and Afa-treated rats at indicated times. Scale bars: 200 μm. (F) Western blot showing lipase levels in dFB-derived adipocytes stimulated by rat skin homogenates. *n*=3 per group. (G) Relative expression of the *Il6* and *Tnfα* mRNAs in HaCaT cells after 4 h of treatment with 100 nM Afa. *n=3* per group. (H) Schematic diagram of the experimental setup used to evaluate the roles of Rosi and adipocytes. (I) Confocal microscopic images of differentiated-dFBs after treatments of HaCaT supernatants from Ctrl, Afa and Afa+Rosi. Lipids were stained with BODIPY 493/503. Scale bars: 50 μm. (J and K) Representative images (J) and quantification (K) of migrated THP-1 cells stimulated with culture media from HaCaT supernatants (Ctrl, Afa, Afa+Rosi)-treated dFB cells. (L) Confocal microscopic images of HaCaT supernatant (Afa)-treated dFBs after treatment with Ctrl or Rosi. Scale bars: 50 μm. (M and N) Representative images (M) and quantification (N) of migrated THP-1 cells stimulated with culture media from HaCaT supernatant (Afa)-treated dFB cells. Then, 5 μM Rosi or vehicle was added to dFBs. (O and

P) Representative images (O) and quantification (P) of migrated THP-1 cells stimulated with culture media from HaCaT supernatant (Afa)-treated undifferentiated or differentiated dFB cells. Data are presented as the means ±SEM. *P < 0.05, **P < 0.01, and ***P < 0.001 (Afa/Rosi group *vs* Ctrl group and Afa+Rosi group *vs* Afa group) using 2-tailed unpaired Student's t test and one-way ANOVA.

To further study how EGFR inhibition promotes adipocyte lipolysis, we performed a direct EGFRI treatment of dFB-derived adipocytes. Unexpectedly, direct treatment of adipocytes with Afa did not increase lipase expression or lipolysis-induced glycerol production (Figure S4G and S4H). In addition, we detected a multitude of small lipid droplets that were newly formed in the isoproterenol group as a positive control, whereas no differences were detected between the Afa-treated and BSA-treated basal groups (Figure S4I). Many studies have reported that the high levels of inflammatory cytokines released during inflammatory diseases increase lipolysis to support the immune response(Feingold et al., 1992). In individuals with EGFRI-induced skin toxicities, the levels of various inflammatory cytokines are increased, including IL6, TNFα and CCL2(Lichtenberger et al., 2013; Mascia et al., 2013). TNFα and IL6 are known to increase lipolysis in adipocytes(Feingold et al., 1992; Pedersen et al., 2003). In contrast, we did not observe differences in the expression of these genes in dWAT cells isolated from the skin of Ctrl- and Afa-treated rats (Figure S4J). However, the treatment of adipocyte homogenates from rat skin revealed obvious upregulation of lipase activity (Figure 4F), thus indicating that cytokines secreted by other skin cells might contribute to lipolysis. According to recent studies, EGFR inhibits or depletes skin epidermal keratinocytes, which express EGFR at high levels, regulating key factors involved in skin inflammation(Lichtenberger et al., 2013; Mascia et al., 2013). We doubted whether epidermal HaCaT cells regulated adipose lipolysis by releasing inflammatory cytokines. Consistent with previous findings, Afa-stimulated HaCaT cells exhibited higher expression levels of *Il6*, but not *Tnfα* (Figure 4G). Notably, the addition of Rosi exerted an obvious inhibitory effect on the transcription of *Il6* (Figure 4G). We designed several coculture experiments to characterize the roles of Rosi and adipocytes in inflammation and lipolysis (Figure 4H). First, we added Afa or Rosi to epidermal HaCaT cells to stimulate or inhibit cytokine transcription, treated differentiated-dFBs with the supernatants from HaCaT cells, and finally collected dFB supernatants for monocyte chemotactic assays. Multiple small lipid droplets formed in the Afa-treated dFB, while larger lipids maintained in the Ctrl and Afa+Rosi group (Figure 4I). The number of migrated monocytes was significantly increased in the Afa group, and migration was suppressed by Rosi (Figure 4J and 4K), indicating that the production of inflammatory cytokines was inhibited by Rosi at the initial stage. Consistent with the transcriptional level, secreted IL6 was increased after Afa treatment both in rat skin homogenates and HaCaT supernatants, and decreased with the addition of Rosi (Figure 4SK and S4L). We next performed the stimulation of IL6 on differentiated-dFB, the lipolysis enhanced by increased level of lipase (Figure S4M), suggesting that the IL6 secreted by keratinocytes induced lipolysis of adipocytes. Activation of PPARγ was reported to stimulate lipid reabsorption, reduce FFA secretion and improve lipid homeostasis(Guan et al., 2002; Sun et al., 2012). To evaluate the direct effect of Rosi on adipocytes during lipolysis, we treated adipocytes with Rosi in the presence of supernatant

from Afa-treated HaCaT cells. The lipid stability was improved with the existence of Rosi (Figure 4L). Although not as significant as the results shown in Figure 4I, the elevated chemotaxis of monocytes was also attenuated by Rosi (Figure 4M and 4N). Given the importance of lipolysis in inflammation, we then dissected whether the participation of adipocytes amplified the inflammatory response. Compared with stimulation of undifferentiated dFBs, the induction of inflammation was remarkable in differentiated dFBs (Figure 4O and 4P). Collectively, these data suggest that the EGFRI induced dermal adipocyte lipolysis, whereas the production of lipolytic cytokines was not induced by the direct stimulation of adipocytes but occurred in keratinocytes. The increased levels of FAs, especially 18:2, induced monocyte migration. Rosi treatment alleviated lipolysis and the inflammatory response by acting on both the epidermis and adipocytes.

Expansion and ablation of dWAT reveal its important roles in the rash process. To directly examine the roles of dermal adipocytes in skin rash during EGFR inhibition while avoiding systemic obese phenotypes or loss of other adipocytes, we established a short-term HFD-induced dWAT expansion model and a pharmacological dWAT ablation model.

Recent reports described the substantial expansion of the dWAT layer in HFD-fed obese mice(Kasza et al., 2016); additionally, increased proliferation of total stromal vascular fraction cells in WAT after long-term HFD feeding and activation of APs at the onset of obesity have been reported(Jeffery et al., 2015). To weaken the metabolic disorders in the obese state, we administered a short-term HFD diet and subsequent EGFRI treatment. Rats fed a HFD for 5 weeks showed an expansion of the dermal adipose layer and a significant increase in the adipocyte size (Figure 5A-5D), while no differences were observed in other adipose depots (Figure 5E), body weight changes (Figure 5F) or systemic serum lipid levels (Figure S5A). We analyzed the expression of general adipogenic genes and AKT signaling in the dFB of rats after 5 weeks of HFD feeding to examine whether AP activation was increased. Significant increases in adipogenesis and AKT phosphorylation were observed (Figure 5G and 5H), verifying an increase in adipogenic ability stimulated by the HFD. Notably, the HFD group showed a reduced occurrence and exacerbation of rash (Figure 5I and 5J; Figure S5B). This result is consistent with a thicker dermal adipose layer and abundant lipid staining (Figure 5K). In addition, rats fed a HFD displayed lower white blood cell, granulocyte and lymphocyte percentages, and the expression of inflammatory receptors was also lower than that in Ctrl-treated rats, suggesting a reduced inflammatory response (Supplementary file 2; Figure S5C).

Deoxycholic acid (DCA) injection is a cytolytic agent approved by the FDA to reduce subcutaneous fat(FDA, 1988). The active ingredient DCA is structurally identical to endogenous deoxycholate, which serves to solubilize dietary diet; therefore, DCA is designed to disrupt the lipid bilayer of cell membranes and induce cell death(Schuller-Petrovic et al., 2008). Based on the function of DCA, we established a dWAT ablation model by administering an intradermal DCA injection. Using female SD rats, we analyzed the effect of DCA after nine total repeated intradermal injections (Figure S6A). Although the thickness of dWAT did not decrease (Figure S6B and S6C), the size of adipocytes was obviously reduced (Figure S6B and S6D). In addition, other skin-related adipocyte depots, such as sWAT, iWAT and BAT, remained unchanged (Figure S6E). After dWAT ablation,

we examined the skin rash process induced by Afa oral gavage in control and DCA rats. The ablation of dWAT didn't affect body weight or food intake (Figure S6F and S6G), but resulted in a moderate deterioration in rash severity after 8 days (Figure S6H-S6J). A routine analysis of white blood cells also showed an elevation in the DCA group (Supplementary file 3). Taken together, we conclude that dermal adipocytes exert potent protective effects on maintaining skin homoeostasis during EGFR inhibition, and the expansion of dWAT is an effective intervention to attenuate skin toxicities. Considering the superficial location of dWAT, a reasonable speculation is that topical application of Rosi would induce the expansion of dWAT, promote AP differentiation and suppress inflammatory cytokine transcription, therefore relieving the skin toxicities of EGFRIs.

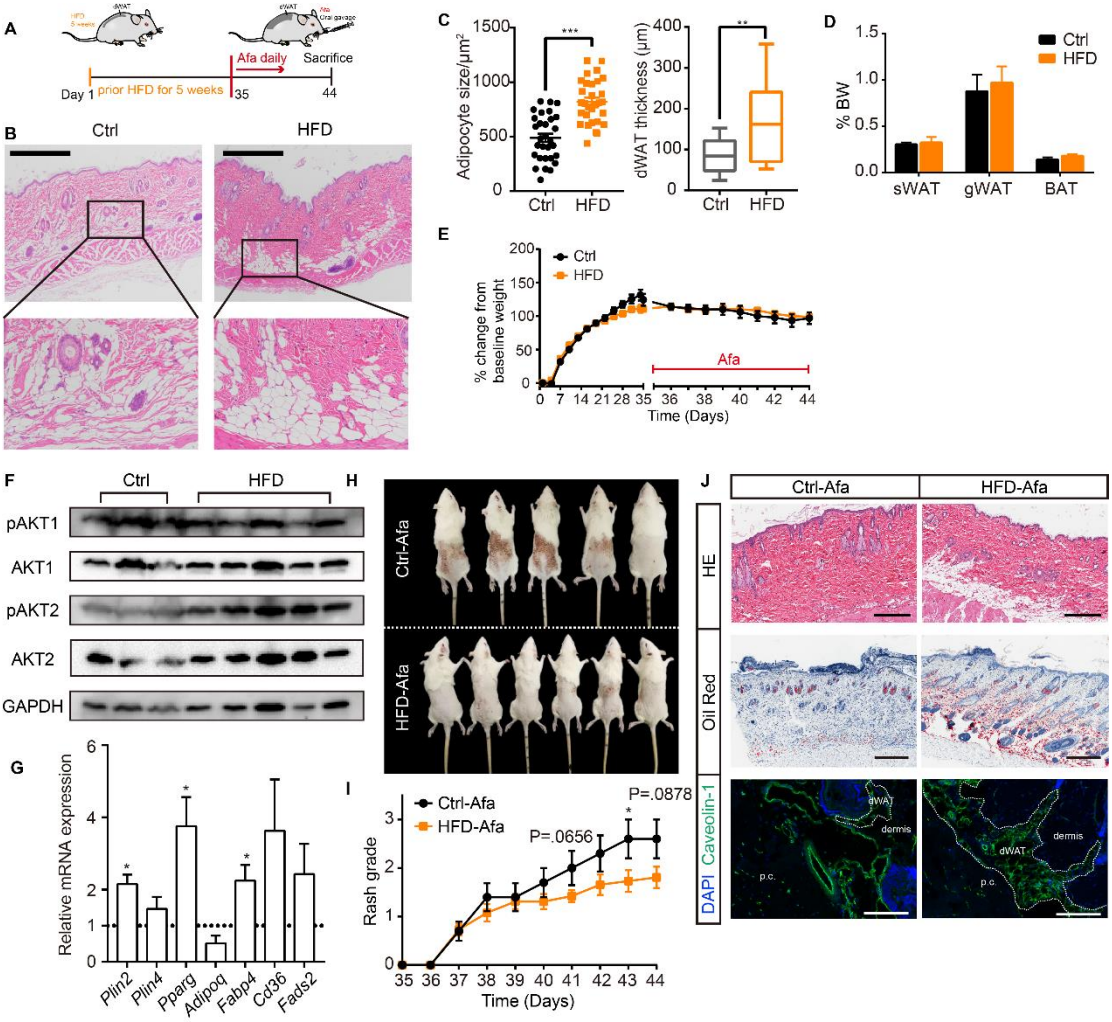

Figure 5 HFD-induced dWAT expansion ameliorates rash phenotypes

(A) Schematic of the strategy used to expand dWAT by the short-term administration of a HFD. (B) H&E staining of skin from normal diet- and HFD-fed rats. Scale bars: 600 μm. (C and D) Size (C) and thickness (D) of dermal adipocytes. (E) Percentage of sWAT, gWAT and BAT relative to BW. (F) Body weight change. (G) Western blot analysis of isolated-dWAT cells (H) Relative mRNA expression of adipogenic genes of isolated-dWAT cells. *n*=5 per group. (I) Photos of the rash at 44 days. (J) Changes in the rash grade after Afa treatment. (K) H&E, Oil Red and Caveolin-1 staining of skin biopsies from Ctrl and HFD rats. Scale bars: 300, 500 and 130 μm (top to bottom). Data are presented as the means ±SEM. *P < 0.05, **P < 0.01, and ***P < 0.001 (HFD group *vs* Ctrl group) using 2-tailed unpaired Student's t test.

582
583 **Prophylactic rosiglitazone application improves the skin phenotype.** We topically
584 applied a Rosi gel and its vehicle gel on shaved backs of rats daily after Afa gavage to
585 assess the prophylactic effect of Rosi on skin toxicity during Afa treatment. Modulating
586 dWAT by the topical application of Rosi gel caused obvious improvements in skin
587 phenotypes (Figure 6A), with a delayed process and low occurrence of rash (Figure 6B
588 and 6C), and improvements in body weight changes (Figure 6D). The architecture of Rosi-
589 treated skin showed fewer neutrophil microcysts, less vascular dilatation and congestion,
590 and more parallel growing hair follicles in anagen phase (Figure 6E-6G). Specifically, the
591 dermal adipocyte layer was still retained in the Rosi group (Figure 6E and 6H). The
592 adipogenic ability recovered, and lipolysis decreased after Rosi treatment (Figure 6I;
593 Figure S7A). Consistent with our previous investigations, the number and mean
594 fluorescence intensity of APs increased after Rosi treatment (Figure S7B-S7D),
595 accompanied by an increased ability to defend against *S. aureus* (Figure 6J). Additionally,
596 the application of Rosi also improved serum lipid levels (Figure S7E).
597 Encouraged by the prophylactic efficacy of Rosi in ameliorating Afa-induced skin
598 toxicity, we next evaluated whether Rosi interferes with the antitumor efficacy of the EGFRI.
599 We topically applied Rosi gel to nude mice subcutaneously receiving PC9 lung carcinoma
600 cells, for which EGFR inhibitors are approved for first-line treatment. After the gavage of
601 Afa, tumor volumes decreased significantly in both the vehicle gel and Rosi gel groups,
602 and the tumor inhibition rates showed no change between vehicle and Rosi groups; in
603 contrast, control mice treated with vehicle displayed rapid tumor growth (Figure S8A-S8D).
604 Intriguingly, Rosi improved body weight and tolerance to Afa (Figure S8E), and mortality
605 occurred in the Ctrl and Afa groups, with six mice in each group. Taken together, these
606 results clearly show that Rosi regulates dWAT to ameliorate EGFRI-associated cutaneous
607 toxicity without interfering with the antitumor effect.
608

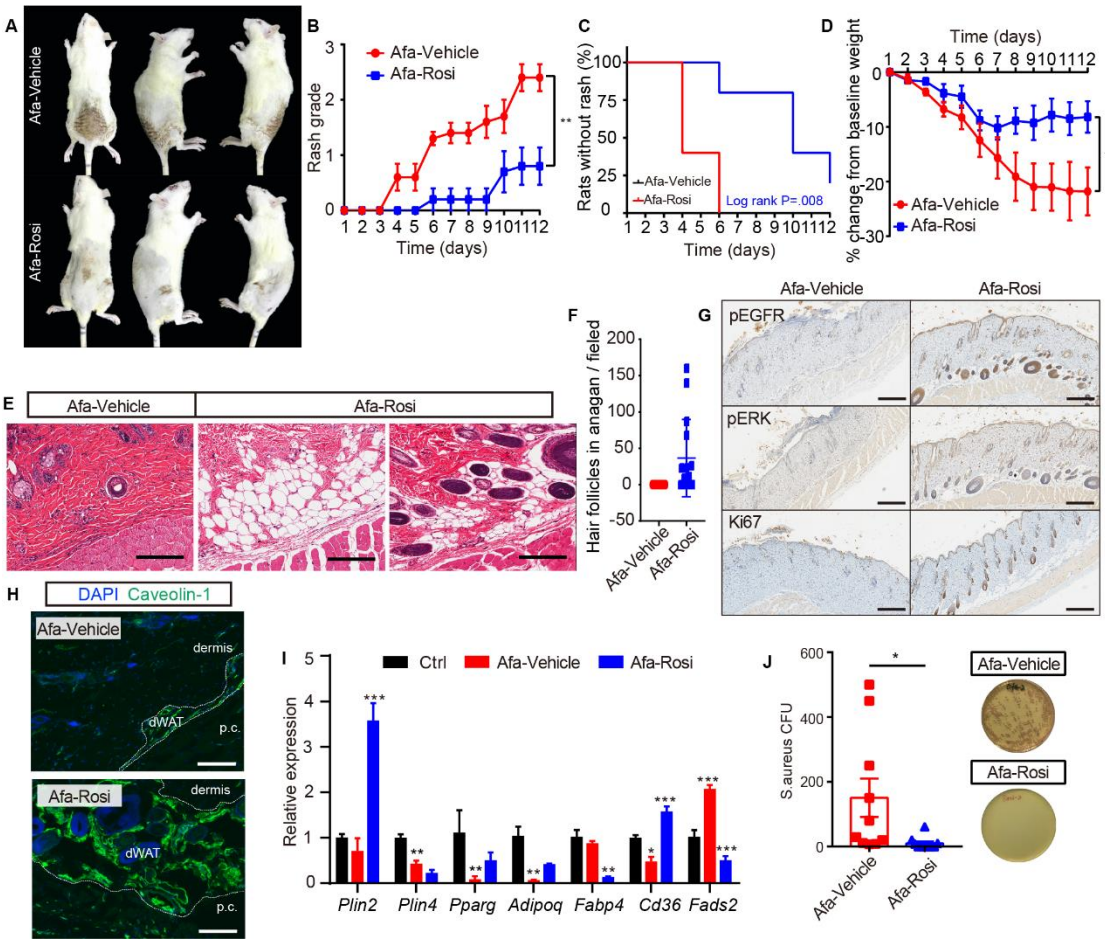

Figure 6 Prophylactic application of Rosi prevents skin toxicities

(A) Representative photos of rash from Vehicle- and Rosi-treated rats. (B) Rash grade. (C) Rash occurrence. (D) Body weight change. (E) H&E staining of skin biopsies. Scale bars: 200 μm. (F) Number of hair follicles in anagen phase. (G) Immunostaining for pEGFR, pERK and Ki67 in skin biopsies from Vehicle- and Rosi-treated rats. *n*=3 per group. Scale bars: 500 μm. (H) Immunostaining for Caveolin-1. Scale bars: 130 μm. (I) Relative expression of adipogenic genes in isolated dWAT cells after Vehicle or Rosi treatment. *n*=3. (J) *S. aureus* growth in media supplemented with skin homogenates from Vehicle- or Rosi-treated rats. *n*= 5 per group. Data are presented as the means ±SEM. *P < 0.05, **P < 0.01, and ***P < 0.001 (Rosi group *vs* Vehicle group) using 2-tailed unpaired Student's t test.

Discussion

Cutaneous toxicities induced by anti-EGFR therapy, in particular rash, are the most frequent adverse effects observed in patients with EGFR-mutant cancers, including non-small cell lung cancer, breast cancer and colorectal cancer. The severity of rash is commonly considered a factor associated with a better prognosis(Peréz-Soler and Saltz, 2005). The pathogenesis of rash is multifactorial. Recent clinical and experimental findings have described EGFRI-induced rash as an inflammatory disease. Several epidermis-targeted genetic mouse models have revealed the relationship of epidermal EGFR with local immune cell activation, keratinocyte differentiation, hair eruption and microbiota outgrowth(Klufa et al., 2019; Lichtenberger et al., 2013; Mascia et al., 2013; Satoh et al.,

2020). Mice lacking EGFR in the epidermis developed the same phenotypes of skin lesions as patients treated with EGFRIs: neutrophilic pustules, initial infiltration of macrophages and mast cells, subsequent T cell infiltration, hair follicle destruction, keratin plugs and bacterial invasion(Mascia et al., 2013). In humans and mice, the recruitment of inflammatory cells is attributed to the production of proinflammatory chemokines such as CCL5 and CCL2(Lichtenberger et al., 2013; Mascia et al., 2013). However, crossing $EGFR^{\Delta ep}$ mice with $CCR2^{-/-}$, $MyD88^{-/-}$, $TNFR^{-/-}$ or $NOS2^{-/-}$ mice did not ameliorate the skin phenotype, while the depletion of macrophages or mast cells only slightly improved the skin phenotype(Lichtenberger et al., 2013; Mascia et al., 2013). These results reveal the complexity of the inflammatory response and various cell-cell interactions following EGFR blockade. The interference of a single cell type or a particular signaling pathway may not be sufficient to explain the abnormal skin phenotypes, which include hair follicles, sebaceous glands, dermal immune cells and blood vessels. Current reports described dermal adipose tissue as a composite tissue maintaining skin functions. dWAT participates in hair cycling, wound healing, thermogenesis, fibrosis and scarring, and immune modulation. Notably, we first noticed that the dWAT layer was diminished in animal models with either genetic EGFR ablation or pharmacological inhibition, and hair follicles were arrested in catagen phase and located far away from the dWAT layer. However, researchers have not determined how dermal adipocytes respond to EGFR inhibition. Moreover, the effect of modulating dWAT on this pathological condition requires further investigation.

Here, we show that a reduction in dermal adipocytes is an early response to EGFR inhibition and leads to the disorder of cutaneous homeostasis. Impaired adipogenesis decreased the skin defense against *S. aureus*, as well as the signaling interactions with hair follicles. In addition, increased migration of monocytes was associated with lipolysis in adipocytes characterized by increased lipase activity. Activation of lipolysis in dermal fat occurs as a response to skin wound repair(Schmidt and Horsley, 2013; Shook et al., 2020). Although macrophages recruited during wound healing by lipolysis were reported to promote revascularization and re-epithelialization(Shook et al., 2020), increased macrophage numbers and free fatty acid contents may also stimulate inflammatory responses via various pattern recognition receptors and cytokine receptors in adipocytes, subsequently inducing cytokine expression and increasing chemoattractant activity(Shi et al., 2006; Wang et al., 2009; Zeng et al., 2018). The infiltration of macrophages in adipose tissue coincided with circulating FFA concentrations and adipose lipolysis, and pharmacologically induced lipolysis by a β3-adrenergic agonist increased macrophage accumulation(Kosteli et al., 2010). Correspondingly, our data also showed a causal relationship among macrophage infiltration, FFA secretion and lipolysis following EGFRI treatment (Figure 4, c, d, Supplementary Figure 4b, c), and the lipids released by disrupting adipocyte cell membranes in the DCA model indicated an accumulation of macrophages (Supplementary Figure 6j). Notably, we showed that dermal adipocytes amplified inflammatory responses from epithelial cells primed with EGFRI treatment. Although epithelial keratinocytes alone secreted chemokines and induced inflammatory infiltration (Supplementary Figure 4), the participation of dermal fat enhanced this process (Figure 4, M and N). The ability of dermal lipids to costimulate keratinocyte-generated cellular

responses represents a novel pathway for the amplification of innate immunity and inflammation. Based on these data, local lipid fluxes are central regulators of the inflammatory response in EGFRI-affected dermal adipose tissue. In this study, we also found a distinction between dermal and subcutaneous white adipose tissue. Although both of these tissues respond early and decrease in size after EGFR inhibition, the expression of adipogenic and fibrotic genes shows different trends; additionally, lipolysis does not occur in subcutaneous fat. These results indicate that the dermal adipose layer is distinct from subcutaneous adipocytes and has a unique role in skin modulation.

Innate immunity of dermal adipose tissue mediated by the release of antimicrobial peptides protects many organs from bacterial infection, such as the skin, peritoneum, endocardium and colon(Dokoshi et al., 2018; Schmid et al., 2017; Zhang et al., 2015). Impaired adipogenesis induced by the PPARγ inhibitors GW9662 and BADGE results in an increased bacterial infection in the skin and colon(Dokoshi et al., 2018; Zhang et al., 2015). Moreover, a recent study observed that retinoids enhance and sustain Camp levels in developing preadipocytes(Liggins et al., 2019). Interestingly, retinoids are therapeutically useful against acne, a disorder driven partly by bacteria(Chivot, 2005). This correlation might also be beneficial to treat acneiform lesions in patients with EGFRI-associated skin disorders. Another skin-related disorder called scarring alopecia is caused by a specific *Pparg* depletion in hair follicle stem cells, and immunohistochemical staining showed proinflammatory lipid and cell accumulation(Karnik et al., 2009). The interplay between dWAT and hair follicles also involves the modulation of the stem cell niche. Follicular stem cell activation was verified to be associated with dermal adipocytes, and hair follicles of mice treated with BADGE or GW9662 did not enter anagen phase and were blocked in telogen phase(Rivera-Gonzalez et al., 2016).

PPARγ acts directly to negatively regulate the expression of inflammatory genes in a ligand-dependent manner by antagonizing the activities of transcription factors, such as members of the NF-κB and AP-1 families. PPARγ stimulation in rodents has been shown to ameliorate several inflammatory diseases, such as atopic dermatitis, psoriasis and acne vulgaris(Ramot et al., 2015). However, previous studies did not obtain evidence of the effect of PPARγ modulation on epidermal functions perturbed by an EGFRI. Here, we show that dWAT plays a critical role in the pathogenesis of cutaneous toxicities induced by EGFR inhibition. Experiments with HFD feeding and DCA injection have shown that dWAT is required to maintain skin homeostasis during EGFR inhibition. Indeed, topical application of rosiglitazone to EGFRI-treated rats prevents the onset of rash and ameliorates the symptoms. Additionally, based on the results obtained from the tumor-bearing nude mice, topical application of rosiglitazone gel did not alter the antitumor effect of afatinib. Therefore, PPARγ agonists may represent a promising new therapeutic strategy in the treatment of EGFRI-related skin disorders.

Acknowledgements

We are grateful to Professor Ling-juan Zhang (School of Pharmaceutical Sciences, Xiamen University, China) for her fruitful discussion. This work was, in part, supported by the Youth Thousand Talents Program of China, start-up grants from the Shanghai Jiao Tong

University (WF220408211). This work was also supported by the grants from the State Key Laboratory of Onco- genes and Related Genes (90-17-02) and from the Interdisciplinary Program of Shanghai Jiao Tong University (YG2017MS18).

Competing interests

No competing interests declared.

Author contributions

L.Y.C. and Q.Y. conceived and designed the study. L.Y.C., Q.Y., M.L., and S.H.L. conducted most of the experiments. Z.Y.W. and J.J.H. performed some of the animal experiments. L.Y.X. analyzed the RNA-seq data. L.Y.C. wrote the manuscript. S.Y.Z. supervised and interpreted experiments, reviewed and edited the manuscript.

References

Bi P, Yue F, Karki A, Castro B, Wirbisky SE, Wang C, Durkes A, Elzey BD, Andrisani OM, Bidwell CA, Freeman JL, Konieczny SF, Kuang S. 2016. Notch activation drives adipocyte dedifferentiation and tumorigenic transformation in mice. *J Exp Med* **213**:2019–2037. doi:10.1084/jem.20160157

Cappuzzo F, Ciuleanu T, Stelmakh L, Cicenas S, Szczésna A, Juhász E, Esteban E, Molinier O, Brugger W, Melezínek I, Klingelschmitt G, Klughammer B, Giaccone G. 2010. Erlotinib as maintenance treatment in advanced non-small-cell lung cancer: A multicentre, randomised, placebo-controlled phase 3 study. *Lancet Oncol* **11**:521–529. doi:10.1016/S1470-2045(10)70112-1

Chen HC, Smith SJ, Tow B, Elias PM, Farese R V. 2002. Leptin modulates the effects of acyl CoA: diacylglycerol acyltransferase deficiency on murine fur and sebaceous glands. *J Clin Invest* **109**:175–181.

Chen SX, Zhang LJ, Gallo RL. 2019. Dermal White Adipose Tissue: A Newly Recognized Layer of Skin Innate Defense. *J Invest Dermatol* **139**:1002–1009. doi:10.1016/j.jid.2018.12.031

Chivot M. 2005. Retinoid therapy for acne. *Am J Clin Dermatol* **6**:13–19.

Deiuliis J, Shah Z, Shah N, Needleman B, Mikami D, Narula V, Perry K, Hazey J, Kampfrath T, Kollengode M. 2011. Visceral adipose inflammation in obesity is associated with critical alterations in tregulatory cell numbers. *PLoS One* **6**:e16376.

Dokoshi T, Zhang LJ, Nakatsuji T, Adase CA, Sanford JA, Paladini RD, Tanaka H, Fujiya M, Gallo RL. 2018. Hyaluronidase inhibits reactive adipogenesis and inflammation of colon and skin. *JCI insight* **3**:1–12. doi:10.1172/jci.insight.123072

Donati G, Proserpio V, Lichtenberger BM, Natsuga K, Sinclair R, Fujiwara H, Watt FM. 2014. Epidermal Wnt/β-catenin signaling regulates adipocyte differentiation via secretion of adipogenic factors. *Proc Natl Acad Sci U S A* **111**. doi:10.1073/pnas.1312880111

FDA. 1988. Center for Drug Evaluation and Pharmacology Review: Secukinumab. *Rev Lit Arts Am* **9**:22–250.

Feingold KR, Doerrler W, Dinarello CA, Fiers W, Grunfeld C. 1992. Stimulation of lipolysis in cultured fat cells by tumor necrosis factor, interleukin-1, and the interferons is blocked by inhibition of prostaglandin synthesis. *Endocrinology* **130**:10–16.

Festa E, Fretz J, Berry R, Schmidt B, Rodeheffer M, Horowitz M, Horsley V. 2011. Adipocyte lineage cells contribute to the skin stem cell niche to drive hair cycling. *Cell* **146**:761–771. doi:10.1016/j.cell.2011.07.019

Guan HP, Li Y, Jensen MV, Newgard CB, Steppan CM, Lazar MA. 2002. A futile metabolic cycle activated in adipocytes by antidiabetic agents. *Nat Med* **8**:1122–1128. doi:10.1038/nm780

Herrmann T, Van der Hoeven F, Gröne H-J, Stewart AF, Langbein L, Kaiser I, Liebisch G, Gosch I, Buchkremer F, Drobnik W. 2003. Mice with targeted disruption of the fatty acid transport protein 4 (Fatp 4, Slc27a4) gene show features of lethal restrictive dermopathy. *J Cell Biol* **161**:1105–1115.

Jeffery E, Church CD, Holtrup B, Colman L, Rodeheffer MS. 2015. Rapid depot-specific activation of adipocyte precursor cells at the onset of obesity. *Nat Cell Biol* **17**:376–385. doi:10.1038/ncb3122

Karnik P, Tekeste Z, McCormick TS, Gilliam AC, Price VH, Cooper KD, Mirmirani P. 2009. Hair follicle stem cell-specific PPARγ deletion causes scarring alopecia. *J Invest Dermatol* **129**:1243–1257. doi:10.1038/jid.2008.369

Kasza I, Hernando D, Roldán-Alzate A, Alexander CM, Reeder SB. 2016. Thermogenic profiling using magnetic resonance imaging of dermal and other adipose tissues. *JCI Insight* **1**:0–13. doi:10.1172/jci.insight.87146

Klufa J, Bauer T, Hanson B, Herbold C, Starkl P, Lichtenberger B, Srutkova D, Schulz D, Vujic I, Mohr T, Rappersberger K, Bodenmiller B, Kozakova H, Knapp S, Loy A, Sibilia M. 2019. Hair eruption initiates and commensal skin microbiota aggravate adverse events of anti-EGFR therapy. *Sci Transl Med* **11**:1–18. doi:10.1126/scitranslmed.aax2693

Kosteli A, Sugaru E, Haemmerle G, Martin JF, Lei J, Zechner R, Ferrante AW. 2010. Weight loss and lipolysis promote a dynamic immune response in murine adipose tissue. *J Clin Invest* **120**:3466–3479. doi:10.1172/JCI42845

Lacouture ME. 2006. Mechanisms of cutaneous toxicities to EGFR inhibitors. *Nat Rev Cancer* **6**:803–812. doi:10.1038/nrc1970

Lichtenberger BM, Gerber PA, Holcmann M, Buhren BA, Amberg N, Smolle V, Schrumpf H, Boelke E, Ansari P, Mackenzie C, Wollenberg A, Kislat A, Fischer JW, Röck K, Harder J, Schröder JM, Homey B, Sibilia M. 2013. Epidermal EGFR controls cutaneous host defense and prevents inflammation. *Sci Transl Med* **5**. doi:10.1126/scitranslmed.3005886

Liggins MC, Li F, Zhang L, Dokoshi T, Gallo RL. 2019. Retinoids Enhance the Expression of Cathelicidin Antimicrobial Peptide during Reactive Dermal Adipogenesis. *J Immunol* **203**:1589–1597. doi:10.4049/jimmunol.1900520

Marangoni RG, Korman BD, Wei J, Wood TA, Graham L V., Whitfield ML, Scherer PE, Tourtellotte WG, Varga J. 2015. Myofibroblasts in murine cutaneous fibrosis originate from adiponectin-positive intradermal progenitors. *Arthritis Rheumatol* **67**:1062–1073. doi:10.1002/art.38990

Mascia F, Lam G, Keith C, Garber C, Steinberg SM, Kohn E, Yuspa SH. 2013. Genetic ablation of epidermal EGFR reveals the dynamic origin of adverse effects of anti-EGFR therapy. *Sci Transl Med* **5**. doi:10.1126/scitranslmed.3005773

Mok TS, Wu Y, Thongprasert S, Yang C, Saijo N, Sunpaweravong P, Han B, Margono B, Ichinose Y, Nishiwaki Y, Ohe Y, Yang J, Chewaskulyong B, Jiang H, Duffield EL, Watkins CL, Armour AA, Fukuoka M. 2017. Gefitinib or Carboplatin–Paclitaxel in Pulmonary Adenocarcinoma. *New Engl J Med* 947–957.

Murillas R, Larcher F, Conti CJ, Santos M, Ullrich A, Jorcano JL. 1995. Expression of a dominant negative mutant of epidermal growth factor receptor in the epidermis of transgenic mice elicits striking alterations in hair follicle development and skin structure. *EMBO J* **14**:5216–5223.

Pedersen BK, Steensberg A, Keller P, Keller C, Fischer C, Hiscock N, Van Hall G, Plomgaard P, Febbraio MA. 2003. Muscle-derived interleukin-6: lipolytic, anti-inflammatory and immune regulatory effects. *Pflügers Arch* **446**:9–16.

Peréz-Soler R, Saltz L. 2005. Cutaneous adverse effects with HER1/EGFR-targeted agents: Is there a silver lining? *J Clin Oncol* **23**:5235–5246. doi:10.1200/JCO.2005.00.6916

Plikus M V., Guerrero-Juarez CF, Ito M, Li YR, Dedhia PH, Zheng Y, Shao M, Gay DL, Ramos R, Hsi TC, Oh JW, Wang X, Ramirez A, Konopelski SE, Elzein A, Wang A, Supapannachart RJ, Lee HL, Lim CH, Nace A, Guo A, Treffeisen E, Andl T, Ramirez RN, Murad R, Offermanns S, Metzger D, Chambon P, Widgerow AD, Tuan TL, Mortazavi A, Gupta RK, Hamilton BA, Millar SE, Seale P, Pear WS, Lazar MA, Cotsarelis G. 2017. Regeneration of fat cells from myofibroblasts during wound healing. *Science (80-)* **355**:748–752. doi:10.1126/science.aai8792

Ramot Y, Mastrofrancesco A, Camera E, Desreumaux P, Paus R, Picardo M. 2015. The role of PPARγ-mediated signalling in skin biology and pathology: New targets and opportunities for clinical dermatology. *Exp Dermatol* **24**:245–251. doi:10.1111/exd.12647

Rivera-Gonzalez GC, Shook BA, Andrae J, Holtrup B, Bollag K, Betsholtz C, Rodeheffer MS, Horsley V. 2016. Skin Adipocyte Stem Cell Self-Renewal Is Regulated by a PDGFA/AKT-Signaling Axis. *Cell Stem Cell* **19**:738–751. doi:10.1016/j.stem.2016.09.002

Satoh TK, Mellett M, Meier-Schiesser B, Fenini G, Otsuka A, Beer HD, Rordorf T, Maul JT, Hafner J, Navarini AA, Contassot E, French LE. 2020. IL-36γ drives skin toxicity induced by EGFR/MEK inhibition and commensal Cutibacterium acnes. *J Clin Invest* **130**:1417–1430. doi:10.1172/JCI128678

Schmid A, Karrasch T, Thomalla M, Schlegel J, Salzberger B, Schäffler A, Hanses F. 2017. Innate Immunity of Adipose Tissue in Rodent Models of Local and Systemic Staphylococcus aureus Infection. *Mediators Inflamm* **2017**. doi:10.1155/2017/5315602

Schmidt BA, Horsley V. 2013. Intradermal adipocytes mediate fibroblast recruitment during skin wound healing. *Dev* **140**:1517–1527. doi:10.1242/dev.087593

Schuller-Petrovic S, Wölkart G, Höfler G, Neuhold N, Freisinger F, Brunner F. 2008. Tissue-toxic effects of phosphatidylcholine/deoxycholate after subcutaneous injection for fat dissolution in rats and a human volunteer. *Dermatologic Surg* **34**:529–543. doi:10.1111/j.1524-4725.2008.34128.x

Sequist L V., Yang JCH, Yamamoto N, O'Byrne K, Hirsh V, Mok T, Geater SL, Orlov S, Tsai CM, Boyer M, Su WC, Bennouna J, Kato T, Gorbunova V, Lee KH, Shah R, Massey D, Zazulina V, Shahidi M, Schuler M. 2013. Phase III study of afatinib or cisplatin plus pemetrexed in patients with metastatic lung adenocarcinoma with EGFR mutations. *J Clin Oncol* **31**:3327–3334. doi:10.1200/JCO.2012.44.2806

Shi H, Kokoeva M V., Inouye K, Tzameli I, Yin H, Flier JS. 2006. TLR4 links innate immunity and fatty acid-induced insulin resistance. *J Clin Invest* **116**:3015–3025. doi:10.1172/JCI28898

Shook BA, Wasko RR, Mano O, Rutenberg-Schoenberg M, Rudolph MC, Zirak B, Rivera-Gonzalez GC, López-Giráldez F, Zarini S, Rezza A, Clark DA, Rendl M, Rosenblum MD, Gerstein MB, Horsley V. 2020. Dermal Adipocyte Lipolysis and Myofibroblast Conversion Are Required for Efficient Skin Repair. *Cell Stem Cell* **26**:880-895.e6. doi:10.1016/j.stem.2020.03.013

Sibilia M, Wagner EF. 1995. Strain-dependent epithelial defects in mice lacking the EGF receptor. *Science* **269**:234–238. doi:10.1126/science.7618085

Sindhu S, Thomas R, Shihab P, Sriraman D, Behbehani K, Ahmad R. 2015. Obesity is a positive modulator of IL-6R and IL-6 expression in the subcutaneous adipose tissue: significance for metabolic inflammation. *PLoS One* **10**:e0133494.

Sugawara K, Schneider MR, Dahlhoff M, Kloepper JE, Paus R. 2010. Cutaneous consequences of inhibiting EGF receptor signaling in vivo: Normal hair follicle development, but retarded hair cycle induction and inhibition of adipocyte growth in EgfrWa5 mice. *J Dermatol Sci* **57**:155–161. doi:10.1016/j.jdermsci.2009.12.004

Sun Xiuhua, Tang Y, Tan X, Li Q, Zhong W, Sun Xinguo, Jia W, McClain CJ, Zhou Z. 2012. Activation of peroxisome proliferator-activated receptor-γ by rosiglitazone improves lipid homeostasis at the adipose tissue-liver axis in ethanol-fed mice. *Am J Physiol - Gastrointest Liver Physiol* **302**:548–557. doi:10.1152/ajpgi.00342.2011

Surguladze D, Deevi D, Claros N, Corcoran E, Wang S, Plym MJ, Wu Y, Doody J, Mauro DJ, Witte L, Busam KJ, Pytowski B, Rodeck U, Tonra JR. 2009. Tumor necrosis factor-α and interleukin-1 antagonists alleviate inflammatory skin changes associated with epidermal growth factor receptor antibody therapy in mice. *Cancer Res* **69**:5643–5647. doi:10.1158/0008-5472.CAN-09-0487

Varga J, Marangoni RG. 2017. Systemic sclerosis in 2016: Dermal white adipose tissue implicated in SSc pathogenesis. *Nat Rev Rheumatol* **13**:71–72. doi:10.1038/nrrheum.2016.223

Wang L, Gill R, Pedersen TL, Higgins LJ, Newman JW, Rutledge JC. 2009. Triglyceride-rich lipoprotein lipolysis releases neutral and oxidized FFAs that induce endothelial cell inflammation. *J Lipid Res* **50**:204–213. doi:10.1194/jlr.M700505-JLR200

Wojciechowicz K, Gledhill K, Ambler CA, Manning CB, Jahoda CAB. 2013. Development of the Mouse Dermal Adipose Layer Occurs Independently of Subcutaneous Adipose Tissue and Is Marked by Restricted Early Expression of FABP4. *PLoS One* **8**:1–15. doi:10.1371/journal.pone.0059811

Wu M, Melichian DS, Chang E, Warner-Blankenship M, Ghosh AK, Varga J. 2009. Rosiglitazone abrogates bleomycin-induced scleroderma and blocks profibrotic responses through peroxisome proliferator-activated receptor-γ. *Am J Pathol* **174**:519–

533.

Zeng J, Zhang Y, Hao J, Sun Y, Liu S, Bernlohr DA, Sauter ER, Cleary MP, Suttles J, Li B. 2018. Stearic Acid Induces CD11c Expression in Proinflammatory Macrophages via Epidermal Fatty Acid Binding Protein. *J Immunol* **200**:3407–3419. doi:10.4049/jimmunol.1701416

Zhang L, Guerrero-juarez CF, Hata T, Bapat SP, Ramos R, Plikus M V, Gallo RL. 2015. Dermal adipocytes protect against invasive Staphylococcus aureus skin infection. *Science (80-)* **347**:67–72.

Zhang L juan, Chen SX, Guerrero-Juarez CF, Li F, Tong Y, Liang Y, Liggins M, Chen X, Chen H, Li M, Hata T, Zheng Y, Plikus M V., Gallo RL. 2019. Age-Related Loss of Innate Immune Antimicrobial Function of Dermal Fat Is Mediated by Transforming Growth Factor Beta. *Immunity* **50**:121-136.e5. doi:10.1016/j.immuni.2018.11.003

Zhang Z, Gupta RK, Scherer PE. 2019. Dermal adipose tissue has high plasticity and undergoes reversible dedifferentiation in mice. *J Clin Invest* **129**:5327–5342.

Supplementary figure legends

Figure S1. Characteristics of sWAT during EGFR inhibition

(A) Body weight change of control and Afa-treated rats. *n*=8 per group. (B) Food intake per rat of different Afa dosage. (C) Percentage of BW change of sWAT, iWAT and BAT. sWAT was obtained under the same shaved-skin area. *n*=3-5 per group. (D) H&E staining of subcutaneous white adipose tissue from Ctrl and Afa-treated rats at indicated time. Scale bars: 300 μm. (E and F) Quantification of the sWAT size (E) and number (F). Data are presented as the means ±SEM. *P < 0.05, **P < 0.01, ***P < 0.001 (Ctrl *vs* Afa) using 2-tailed unpaired Student's t test.

Figure S2. Additional dedifferentiation changes of dWAT and sWAT

(A and B) mRNA levels of pro-fibrotic and pro-adipogenic genes in sWAT at one day before (A), and one day after rash (B), *n*=3 per group. (C) PDGFRα (green) and DAPI (bule) immunostaining of dedifferentiated adipocytes under Afa treatment at day 9. Data are presented as the means ±SEM. *P < 0.05, **P < 0.01, ***P < 0.001 (Ctrl *vs* Afa) using 2-tailed unpaired Student's t test.

Figure S3. Expression levels of inflammatory receptors during dFB differentiation

(A) Viability of dFB cells under different Afa concentrations. (B) mRNA levels of IL4R, CCR2, IL6R, TNFR, and TLR2-3 of differentiating dFB with Afa (10 nM) or Rosi (5 μM) treatment. *n*=4 per group. Data are presented as the means ±SEM. *P < 0.05, **P < 0.01, ***P < 0.001 (Afa/Rosi *vs* Ctrl, Afa+Rosi *vs* Afa) using 2-tailed unpaired Student's t test and one-way ANOVA.

Figure S4. Lipolytic effects of direct EGFRI stimulation on adipocytes

(A) Glycerol concentration after 2h ISO or Afa treatment.on isolated sWAT at indicated times. *n*=3-5. (B and C) Lipid mass spectrometry quantification of medium- and long-free fatty acids. *n*=6 per group. SFA: saturated fatty acid . MUFA: monounsaturated fatty acid.

PUFA: polyunsaturated fatty acid. (D) FFA concentration of differentiated-dFBs after treatments of HaCaT supernatants from Ctrl, Afa and Afa+Rosi. *n*=3. (E) Quantification of migrated THP-1 cells after stimulation by different FAs. (F) Representative images of migrated THP-1 cells treated with different concentrations of 18:2 FA. Scale bars: 30 μm. (G) Western-blotting of lipase in dFB-derived adipocytes stimulated by 10 μM ISO or 100 nM Afa. (H) Glycerol concentration after 2h ISO or Afa treatment on isolated dWAT. *n*=3. (I) Confocal microscopic images of differentiated dFB cells in basal, ISO and Afa treatment. Lipids were stained with BODIPY 493/503. (J) Relative mRNA expression of *Il6*, *Ccl2* and *Tnfα* in isolated dWAT. *n*=3 per group. (K) IL6 levels in skin homogenates from Ctrl- and Afa-treated rats. *n*=9-10. (L) IL6 levels in HaCaT supernatants after Ctrl, Afa or Afa+Rosi treatment. *n*=5. (M) Western-blotting of lipase in differentiated-dFB stimulated by Ctrl or IL6. Data are presented as the means. *P < 0.05, **P < 0.01, ***P < 0.001 using 2-tailed unpaired Student's t test.

Figure S5. Additional characterization of HFD rats

(A) Serum lipid of Ctrl and HFD rats. APO-B refers to apolipoprotein B, HDL-C refers to high-density lipoproteincholesterol, LDL-C refers to low-density lipoproteincholesterol, TC refers to total cholesterol, TG refers to triglyceride. *n*=3 per group. (B) Left and right photos of rash from Ctrl and HFD rats. (C) Relative expression of inflammatory receptors in dFB assayed by RT-PCR from rats at day 35 and day 44. *n*=5 per group. Data are presented as the means ±SEM. *P < 0.05 using 2-tailed unpaired Student's t test.

Figure S6. DCA-induced dWAT ablation aggravates rash phenotypes

(A) Schematic of the strategy to ablate dWAT by repeatedly DCA intradermal injection. (B) H&E staining of skin from Vehicle and DCA rats. Scale bars: 300 μm. (C and D) Size (C) and thickness (D) of dermal adipocytes. (E) Percentage of BW of sWAT, gWAT and BAT. (F) Body weight. (G) Food intake. (H) Rash grade. (I) Photos of rash at 40 days. (J) Oil Red, Caveolin-1 and CD68 staining of skin biopsies from Ctrl and DCA rats at day 40. Scale bars: 500, 130 and 200 μm (top to down). Data are presented as the means ±SEM. ***P < 0.001 using 2-tailed unpaired Student's t test.

Figure S7. Additional effects of Rosi prevention in Afa-treated rats

(A) Western-blotting of lipase in dFB-derived adipocytes stimulated by rat skin homogenates. *n*=3 per group. (B) FACS analysis of APs. (C) Quantification of APs. (D) Mean fluorescence intensity (MFI) of CD29 and CD34. (E) Serum lipid of Ctrl, Afa-Vehicle and Afa-Rosi groups. GLU refers to glucose, HDL-C refers to high-density lipoproteincholesterol, LDL-C refers to low-density lipoproteincholesterol, LP (a) refers to lipoprotein (a), TC refers to total cholesterol, TG refers to triglyceride. *n*=5 per group. Data are presented as the means ±SEM. P < 0.05, **P < 0.01, ***P < 0.001 (Ctrl/Rosi *vs* Afa) using one-way ANOVA.

Figure S8. Rosi did not interfere the anti-tumor effect of EGFRI

Ctrl: mice gavaged with solvent. Afa 30 mpk (mg/kg): Mice were gavaged with Afa and topically administered vehicle gel. Afa 30 mpk+Rosi: Mice gavaged with Afa and topically

977 administered Rosi gel. (A) Tumor volume. (B and C) Photos of nude mice (B) and tumors
978 (C) at day 10. (D) Tumor inhibition. (E) Body weight. *n*=4-6 per group. Data are presented
979 as the means ±SEM. P < 0.05, **P < 0.01, ***P < 0.001 (Ctrl/Afa+Rosi *vs* Afa) using one-
980 way ANOVA.